Abdominal Radiology (2021) 46:1864–1875
https://doi.org/10.1007/s00261-020-02801-2

HEPATOBILIARY

Noninvasive DW-MRI metrics for staging hepatic fibrosis and grading inflammatory activity in patients with chronic hepatitis B

Fangfang Fu[1] · Xiaodong Li[1] · Qiuyu Liu[2] · Cuiyun Chen[1] · Yan Bai[1] · Dapeng Shi[1] · Jia Sang[3] · Kaiyu Wang[4] · Meiyun Wang[1]

Received: 11 July 2020 / Revised: 21 September 2020 / Accepted: 29 September 2020 / Published online: 19 October 2020

Abstract

Purpose To assess the value of various diffusion parameters obtained from monoexponential, biexponential, and stretched-exponential diffusion-weighted imaging (DWI) models for staging hepatic fibrosis (HF) and grading inflammatory activity in patients with chronic hepatitis B (CHB).

Methods 82 patients with CHB and 30 healthy volunteers underwent DWI with 13 *b*-values on a 3T MRI unit. The standard apparent diffusion coefficient (ADC_{st}) was calculated using a monoexponential model. The true diffusion coefficient (D_t), pseudo-diffusion coefficient (D_p), and perfusion fraction (f) were calculated using a biexponential model. The distributed diffusion coefficient (DDC) and water-molecule diffusion heterogeneity index (α) were calculated using a stretched-exponential model. Receiver operating characteristic (ROC) curves were performed for diffusion parameters to compare the diagnosis performance.

Results The distributions of hepatic fibrosis stages and the inflammatory activity grades (METAVIR scoring system) were as follows: F0, $n=1$; F1, $n=16$; F2, $n=31$; F3, $n=19$; and F4, $n=15$. A0, $n=1$; A1, $n=14$; A2, $n=46$; and A3, $n=21$. ADC_{st}, D_t and DDC values showed negative correlation with the fibrosis stage ($r=-0.418$, -0.717 and -0.630, all $P<0.001$) and the inflammatory activity grade ($r=-0.514$, -0.626 and -0.550, all $P<0.001$). The area under the ROC curve (AUC) of D_t (AUC = 0.854, 0.881) and DDC (AUC = 0.794, 0.834) were significantly higher than that of ADC_{st} (AUC = 0.637, 0.717) in discriminating significant fibrosis (≥ F2) and advanced fibrosis (≥ F3) (all $P<0.05$). Although D_t (AUC = 0.867, 0.836) and DDC (AUC = 0.810, 0.808) showed higher AUCs than ADC_{st} (AUC = 0.767, 0.803), there was no significant difference in their ability in detecting inflammatory activity grade ≥ A2/A3 ($P > 0.05$).

Conclusions D_t and DDC are promising indicators and outperform ADC_{st} for staging HF. While both D_t and DDC have similar diagnostic performance compared with ADC_{st} for grading inflammatory activity.

Keywords Diffusion magnetic resonance imaging · Liver · Fibrosis · Liver cirrhosis · Hepatitis B · Chronic

Introduction

Chronic hepatitis B (CHB) virus infection could cause damage to the hepatic parenchyma, leading to hepatic fibrosis (HF) [1–3]. Moreover, the progression of untreated HF may eventually cause cirrhosis, and subsequently hepatocellular carcinoma (HCC). Recent clinical studies have revealed that the use of anti-fibrotic drugs in patients with CHB in the early stages of HF may result in reversal of HF [4]. Therefore, early detection and stratification of HF is critical. Currently, invasive liver biopsy is the gold standard for evaluating HF [5, 6], but this technique has some potential limitations including sampling errors and inter-observer variations [5, 7]. Hence, reliable and

Fangfang Fu and Xiaodong Li have contributed equally to this work.

✉ Meiyun Wang
mywang@ha.edu.cn

1 Department of Medical Imaging, Henan Provincial People's Hospital & People's Hospital of Zhengzhou University, 7 Weiwu Road, Zhengzhou 450003, Henan, China

2 Department of Pathology, Henan Provincial People's Hospital, Zhengzhou 450003, Henan, China

3 Department of Infectious Diseases, Henan Provincial People's Hospital, Zhengzhou 450003, Henan, China

4 Department of MR Research China, GE Healthcare, Beijing 100000, China

noninvasive methods are essential for early detecting and staging of HF.

Diffusion-weighted imaging (DWI) is a noninvasive technique based on the Brownian motion of water molecules in biological tissue and has shown potential in the assessment of HF [8, 9]. The ADC_{st} parameter obtained from monoexponential DWI model has been used for the detection and semiquantification of HF and has shown promise in HF evaluations [6, 8, 10]. However, ADC_{st} values may not accurately represent water-molecule diffusion because they are influenced by the microcirculation of blood in the capillaries.

Some previous studies have proposed that biexponential or stretched-exponential DWI models may provide more accurate information with respect to water diffusion [11–20]. The biexponential intravoxel incoherent motion (IVIM) model, which was introduced by Le Bihan et al. [11], could generate three parameters including D_p (representing capillary perfusion), D_t (representing true water molecular diffusion), and f (reflecting the fractional volume of blood flowing in the capillaries) [11], and hence could allow separation of water-molecule diffusion from microcirculation in vivo. The stretched-exponential model proposed by Bennett et al. [12] could generate two parameters including DDC (representing the mean intravoxel diffusion rate), and α (representing the intravoxel water diffusion heterogeneity), and hence could truly reflect the physiological characteristics of tissue in vivo. All the diffusion parameters can be derived from the post-reconstruction of multi-b value DWI. But the efficiency of these parameters in different reconstruction models need further exploration.

Since various diffusion parameters obtained from different DWI models may display different aspects of biological tissue, a thorough investigation and comparison of their roles in evaluating HF and inflammation may be valuable. Although some earlier studies [6, 8–11, 16, 18–20] have explored the value of monoexponential and biexponential DWI models in evaluation of HF from various etiologies, the degree and pattern of HF may be variable with different etiologies of chronic hepatic disease. To our knowledge, however, no study has compared various diffusion parameters obtained from monoexponential, biexponential, and stretched-exponential DWI models in the assessment of HF and inflammatory activity in CHB. Therefore, this study aimed to explore and compare the effectiveness of the diffusion parameters obtained from monoexponential, biexponential, and stretched-exponential models in evaluation of HF and inflammatory activity in patients with CHB.

Materials and methods

Study population

This prospective study was approved by the institutional review board, and informed consent was obtained from all participants. A total of 102 patients with chronic HBV infection were recruited consecutively and underwent liver magnetic resonance (MR) examinations (including routine sequences and DWI with multiple b-values) between June 2014 and December 2016. The inclusion criteria were as follows: (a) MR imaging was performed prior to liver biopsy, and the interval between MR imaging and liver biopsy was less than one month; (b) pathological results were obtained; (c) the patients had no surgical history involving the right lobe of the liver. The exclusion criteria were as follows: (a) MR data were not available due to respiratory artefacts; (b) patients had other focal lesions in the liver. Based on the exclusion and inclusion criteria, 20 patients were excluded from the study for the following reasons: four did not undergo liver biopsy, six had poor images with artefacts, four had other lesions, and six had fatty liver disease. Consequently, a total of 82 patients (55 males and 27 females; mean age: 36.7 years, age range: 22–61 years) were included in this study (Fig. 1). Concomitantly, 30 healthy subjects (8 males and 22 females, mean age: 31.3 years, age range: 22–69 years) with no history of liver disease, alcohol abuse, liver dysfunction, and liver biopsy were enrolled as the control group (Fig. 1). All the healthy subjects had undergone liver MR examinations.

Image data acquisition

All patients underwent liver MR on a 3T MR imaging unit (Discovery MR750; GE Medical System, Milwaukee, WI, USA) with an eight-channel phased-array coil (GE Medical Systems). All patients fasted for at least 8 h before the MR examinations. They underwent a routine liver MRI sequence, which consisted of an axial T1-weighted fast spin-echo sequence (repetition time [TR]/echo time [TE], 180 ms/2.1 ms), and an axial T2-weighted fast spin-echo sequence with fat suppression (TR/TE, 4800 ms/76 ms).

DWI with multiple b-values was performed using a respiratory-triggered single-shot spin-echo planar sequence with the parallel imaging technique and a monopolar gradient in the axial plane. DWI with multiple b-values used the following parameters: TR/TE, 9230 ms/minimum; slice thickness, 5 mm; gap, 1 mm; field of view, 360 mm × 380 mm; and matrix, 128 × 128. Thirteen b-values from 0 to 2000s/mm^2 (0, 50, 100, 150, 200, 300, 500, 800, 1000, 1300, 1500, 1700, and 2000 s/mm^2) were used for performing DWI in three diffusion directions.

Data analysis

Images were obtained and transferred to a workstation (Advantage Workstation 4.6; GE Medical Systems) for processing. They were independently processed and analysed

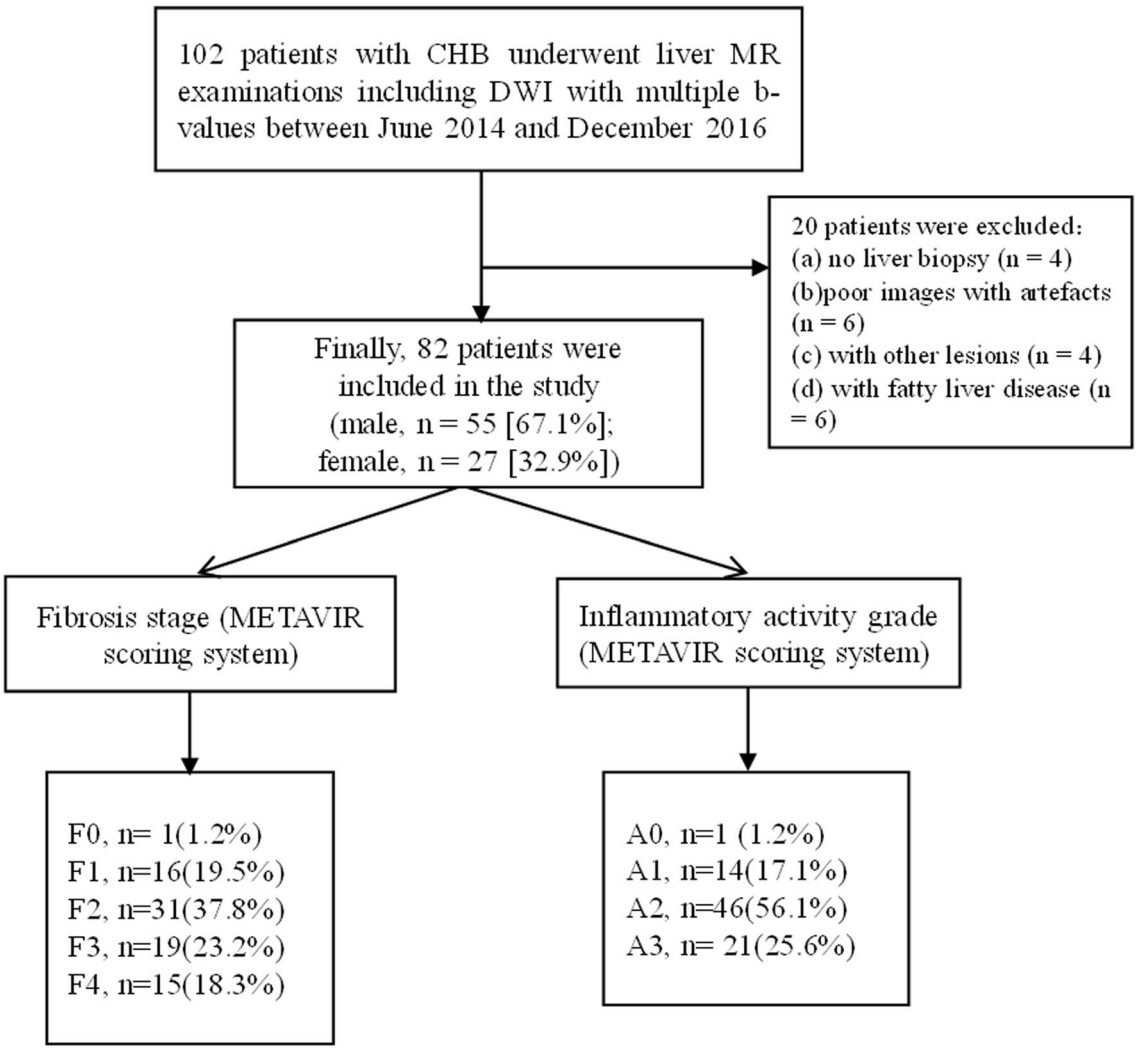

Fig. 1 Flowchart of the patient evaluation process

by two experienced radiologists who were blinded to the histopathologic results.

The ADC_{st} value was calculated from all 13 *b*-values with a monoexponential model as follows [13]:

$$S(b)/S(0) = \exp(-b \times \mathrm{ADC})$$

where $S(b)$ represents the signal intensity in the presence of diffusion sensitisation, $S(0)$ represents the signal intensity in the absence of diffusion sensitisation, b represents the diffusion sensitising factor, and ADC represents an apparent diffusion coefficient.

The true diffusion coefficient (D_t), pseudo-diffusion coefficient (D_p), and perfusion fraction (f) were calculated with the biexponential model as follows [13]:

$$S(b)/S(0) = \left[(1-f) \times \exp\left(-b \times D_t\right)\right] + \left[f \times \exp\left(-b \times D_p\right)\right],$$

The water-molecule diffusion heterogeneity index (a) and the distributed diffusion coefficient (DDC) were obtained using a stretched-exponential model that employed the following equation [12]:

$$S(b)/S(0) = \exp\left(-b \times DDC\right)^{\alpha},$$

where α varies between 0 and 1, which represents the intravoxel water-molecule diffusion heterogeneity. A numerically high value characterises low intravoxel diffusion heterogeneity, which approaches the monoexponential decay. The index DDC represents the mean intravoxel diffusion rate.

For every patient, the two radiologists independently placed three regions of interest (ROIs) in the right lobe of the liver on the ADC_{st} maps to acquire measurements and calculated the mean values. The areas of the ROIs varied from 150 to 200 mm^2, and the ROIs were selected avoiding large vessels and bile ducts to ensure more accurate

measurements [21]. The selected ROIs were copied to the maps of the other parameters (D_t, D_p, f, DDC, and α) from the same patient.

Histopathological analysis

Liver biopsy specimens from the right lobe of the liver were analysed independently by two experienced pathologists. The METAVIR scoring system was used to semi-quantitatively evaluate fibrosis and inflammation [22]. The degree of fibrosis was staged as follows: F0 = no fibrosis, F1 = portal fibrosis without septa formation, F2 = portal fibrosis with few septa, F3 = numerous septa without cirrhosis, and F4 = cirrhosis. The inflammation activity was graded as follows: A0 = no activity, A1 = mild activity, A2 = moderate activity, and A3 = severe activity. Any cases in which the final fibrosis stage or activity grade differed between the two pathologists were reevaluated and scored in consensus.

Statistical analysis

All analyses were performed using IBM SPSS 23.0(SPSS, Chicago, IL) and MedCalc 12.0 (Mariakerke, Belgium). The mean results for each parameter (ADC_{st}, D_t, D_p, f, DDC, and α) were utilised for quantitative statistical analyses. The Kruskal–Wallis H test was employed for comparisons of each parameter among the control and the fibrosis stage groups, or the control and inflammatory activity grade groups. The Mann–Whitney U test was adopted to compare each parameter between the fibrosis stage ≤ F1 and ≥ F2, between stage ≤ F2 and ≥ F3, between stage ≤ F3 and F4. Additionally, the Mann–Whitney U test was adopted to compare each parameter between the inflammatory activity grade ≤ A1 and ≥ A2, between grade ≤ A2 and A3. Spearman rank correlation was adopted to evaluate the correlation of each parameter with fibrosis stages and inflammatory activity grades. ROC curves were performed for all parameters to assess the AUC and to establish which parameter was optimal for predicting fibrosis stages and inflammatory activity grades. The inter-observer agreement for the two independent quantitative analyses was evaluated by calculating the intraclass correlation coefficient. Results with P values < 0.05 were considered significantly different.

Results

Histological quantification of fibrosis stage and inflammatory activity grade was performed in 82 patients with CHB by liver biopsy. The fibrosis stage distribution is as follows (Fig. 1): F0, $n = 1$; F1, $n = 16$; F2, $n = 31$; F3, $n = 19$; and F4, $n = 15$. The inflammatory activity grade distribution is as follows: A0, $n = 1$; A1, $n = 14$; A2, $n = 46$; and A3, $n = 21$.

Figure 2 shows the DWI and ADC_{st}, D_t, D_p, f, DDC, and α maps for a patient with fibrosis stage 2 and inflammatory activity grade 2. All parameters except D_p and α were significantly different among the control group and groups F1, F2, F3, and F4 (all $P < 0.001$) and showed a tendency to decrease gradually as the HF stage progressed (Fig. 3). Additionally, all parameters except D_p and α were significantly different among the control group and groups A1, A2, and A3 (all $P < 0.001$) and showed a tendency to decrease gradually as the inflammatory activity grade progressed (Fig. 4).

ADC_{st}, D_t and DDC values showed moderately negative correlation with the fibrosis stage ($r = -0.418$, -0.717 and -0.630, all $P < 0.001$). The ADC_{st}, D_t, f, and DDC values were significantly lower in fibrosis stage ≥ F2 than stage ≤ F1 (all $P < 0.05$), significantly lower in fibrosis stage ≥ F3 than stage ≤ F2, and significantly lower in fibrosis stage F4 than stage ≤ F3 (all $P < 0.05$) (Table 1). However, D_p and α values showed no significant differences in these comparisons ($P < 0.05$).

For the evaluation of fibrosis stages (≥ F2/ ≥ F3/F4), D_t and DDC showed the higher diagnostic value than ADC_{st} (all $P < 0.05$), with an exception that both D_t and DDC showed a similar diagnostic performance to ADCst in detecting stage F4 (Fig. 5, Table 2). Moreover, D_t and DDC showed a comparable diagnostic performance in detecting fibrosis stage ≥ F2/ ≥ F3/F4.

Moreover, ADC_{st}, D_t and DDC values showed moderately negative correlation with the inflammatory activity grade ($r = -0.514$, -0.626 and -0.550, all $P < 0.001$). The ADC_{st}, D_t, f, and DDC values were significantly lower in inflammatory activity grade ≥ A2 than in grade ≤ A1 (all $P < 0.05$), and significantly lower in inflammatory activity grade A3 than in grade ≤ A2 (all $P < 0.05$). D_p and α values showed no significant differences in the above comparisons (all $P > 0.05$) (Table 3).

For the evaluation of inflammatory activity grades (≥ A2/A3), although D_t and DDC showed higher AUCs than ADC_{st}, there were no significant differences between the diagnostic performance of D_t and ADC_{st} or between the diagnostic performance of DDC and ADC_{st} (all $P > 0.05$) (Fig. 6, Table 4). Moreover, D_t and DDC showed a comparable diagnostic performance in detecting inflammatory activity grade ≥ A2/A3.

The overall mean interclass correlation coefficient between the two independent radiologists was 0.871 ($P < 0.001$).

Discussion

In the study, we observed that the D_t, DDC and ADC_{st} values were significantly lower in ≥ F2 than in ≤ F1, lower in ≥ F3 than in ≤ F2, lower in ≥ A2 than in ≤ A1 and lower in A3

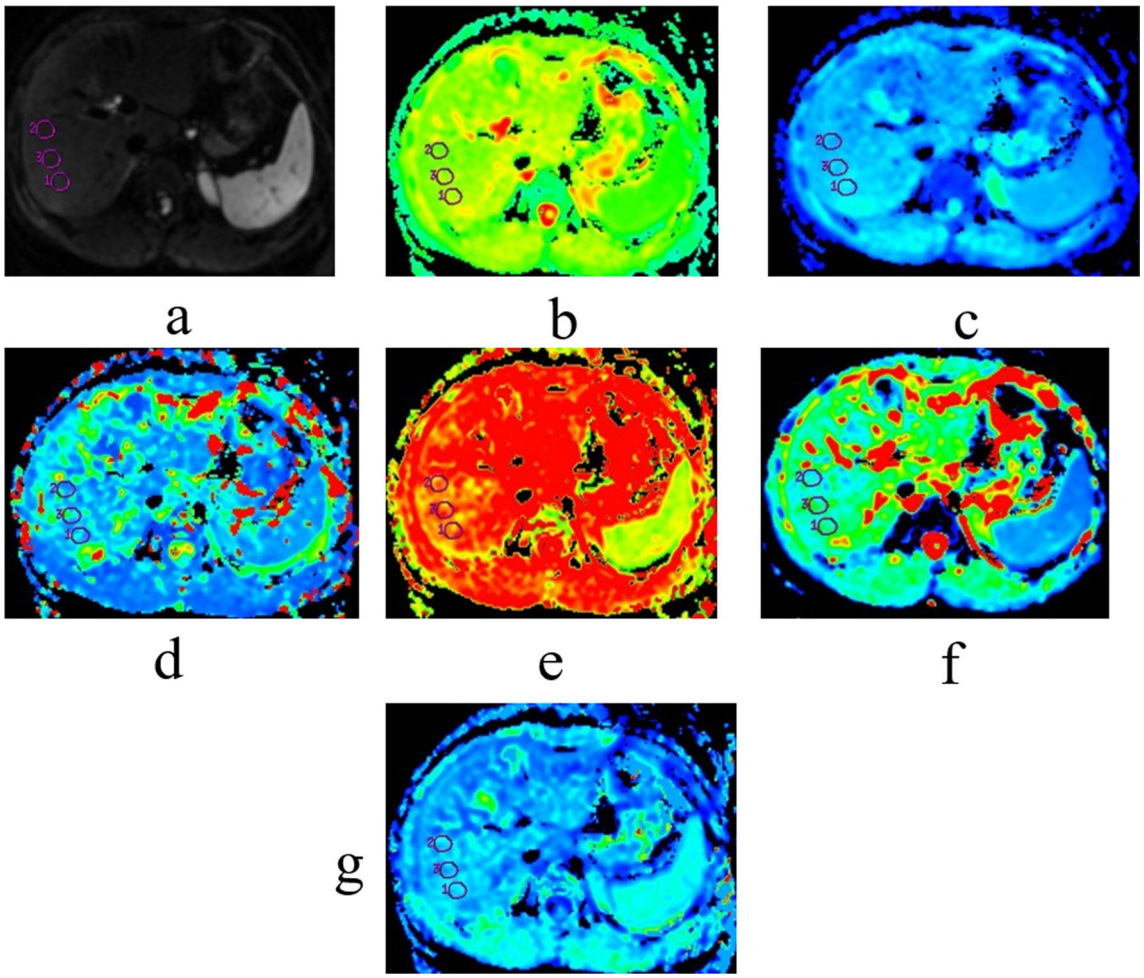

Fig. 2 A 26-year-old female patient with CHB with fibrosis stage 2 and inflammatory activity grade 2. Diffusion-weighted image with $b=50$ s/mm^2 (**a**). The ADC_{st} map showed that the ADC_{st} value was 0.92×10^{-3} mm^2/s (**b**). The D_t map showed that the D_t value was 0.67×10^{-3} mm^2/s (**c**). The D_p map showed that the D_p value was 24×10^{-3} mm^2/s (**d**). The f map showed that the f value was 25.9% (**e**). DDC map showed that the DDC value was 1.02×10^{-3} mm^2/s (**f**). The α map showed that the α value was 0.70 (**g**)

than in ≤ A2. In addition, D_t and DDC had higher diagnostic performances than ADC_{st} in detecting fibrosis stage ≥ F2, stage ≥ F3. Nevertheless, D_t, DDC and ADC_{st} had similar diagnostic performance for discriminating inflammatory activity grade ≥ A2 and grade A3. Hence, D_t and DDC are optimal diffusion parameters for evaluation of HF in CHB in comparison with the other diffusion parameters.

Thus, these results indicate that the ADC_{st}, D_t and DDC values in the fibrosis stage groups (F1/F2/F3/F4) were significantly lower than the corresponding values in the control group. The parameter ADCst obtained from mono-exponential DWI model is usually used to reflect water diffusion, however, it was unable to separate the water diffusion from the microcirculation perfusion [6, 8–10]. The diffusion-related D_t obtained from the biexponential DWI model reflects the true water diffusion with a slower flow and is measured with b-values higher than 200 s/mm^2 [11, 13, 15–20]. DDC obtained from the stretched-exponential DWI model for represents the mean intravoxel diffusion rate [12]. The limitation of water molecules diffusion can lead to the reduced ADC_{st}, D_t and DDC values. The limitation of water molecules diffusion in the fibrotic liver could be attributed to the following aspects of HF pathogenesis: HF is associated with excessive synthesis and sedimentation of the extracellular matrix, specifically in collagen fibres, in which the protons are less abundant and tightly bound [23]. The existence of collagen fibres in the distorted lobular tissue would therefore limit water-molecule diffusion in the fibrotic liver, resulting in decreased ADC_{st}, D_t and DDC values. Several prior studies [6, 24, 25] have reported that the ADC_{st} and D_t values obtained using with multiple b-values in HF and cirrhosis were lower than those in the normal liver. Our study results accord with these prior study results. Regarding the diagnosis of HF with DDC values, Anderson

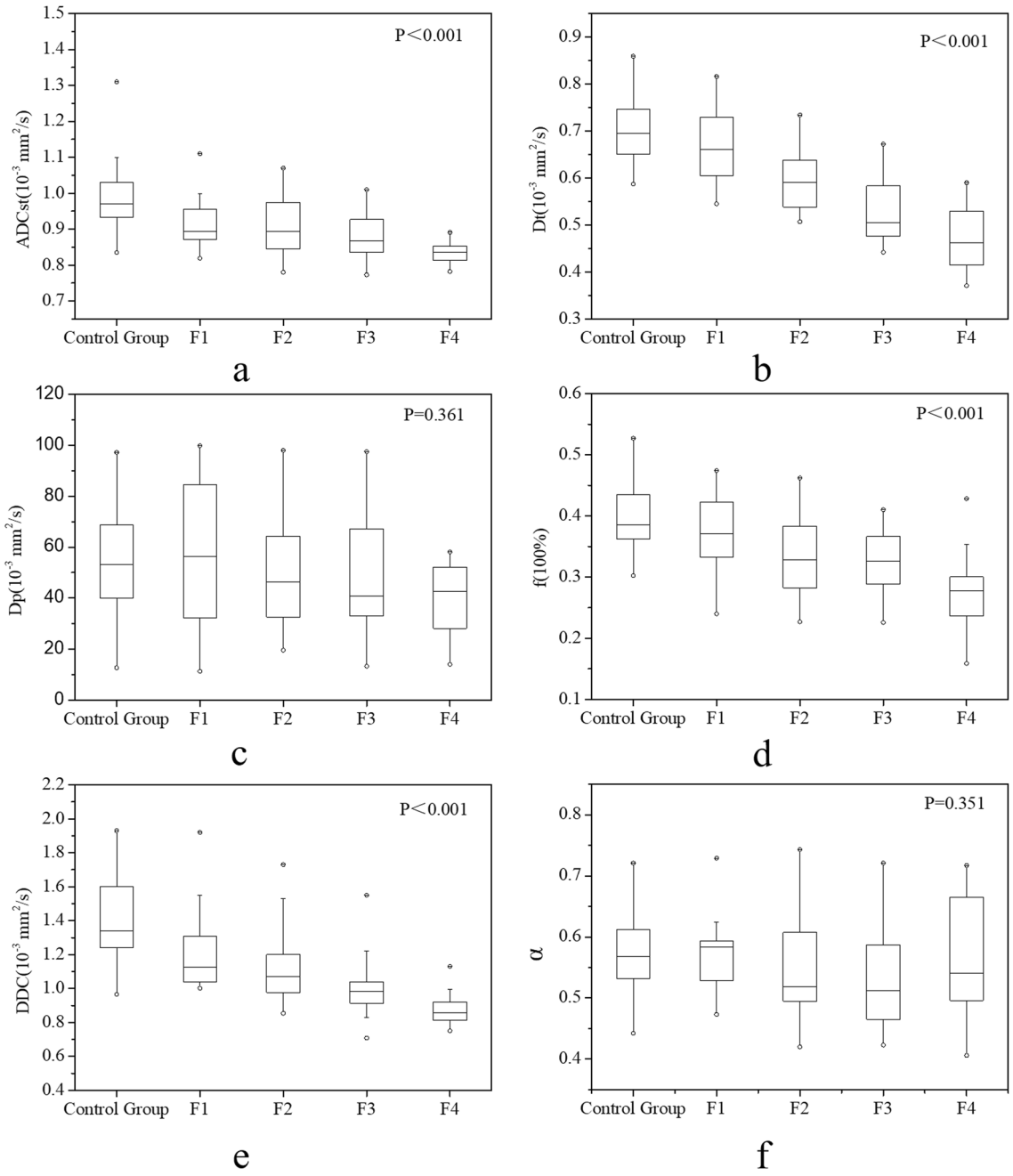

Fig. 3 Box plots of ADC_{st} values (**a**), D_t values (**b**), D_p values (**c**), f values (**d**), DDC values (**e**), and α (**f**) values for the control group and groups F1, F2, F3, and F4. ADCst, D_t, f, and DDC values were significantly different among the above groups (all $P<0.001$). However, D_p and α values did not show significant differences (all $P>0.05$)

et al. [26] has reported by using an ex vivo murine that DDC values in the HF group were significantly lower than those in the control group. Our study result is consistent with the previous study. In this study, the α values showed no significant differences among the HF groups and the control group, which is also in good agreement with the findings of the prior study by Anderson et al. [26]. Thus, the stretched-exponential model showed no clear evidence of an increase in intravoxel heterogeneity of HF in comparison with the normal liver.

It is well known that HF is associated with decreased liver perfusion. The increased arterial flow activated by intrahepatic portal hypertension in HF is inadequate to compensate for the decreased portal flow. Both D_p and f from the biexponential DWI model were perfusion-related parameter [11, 13, 27]. D_p is used for evaluating microcapillary perfusion

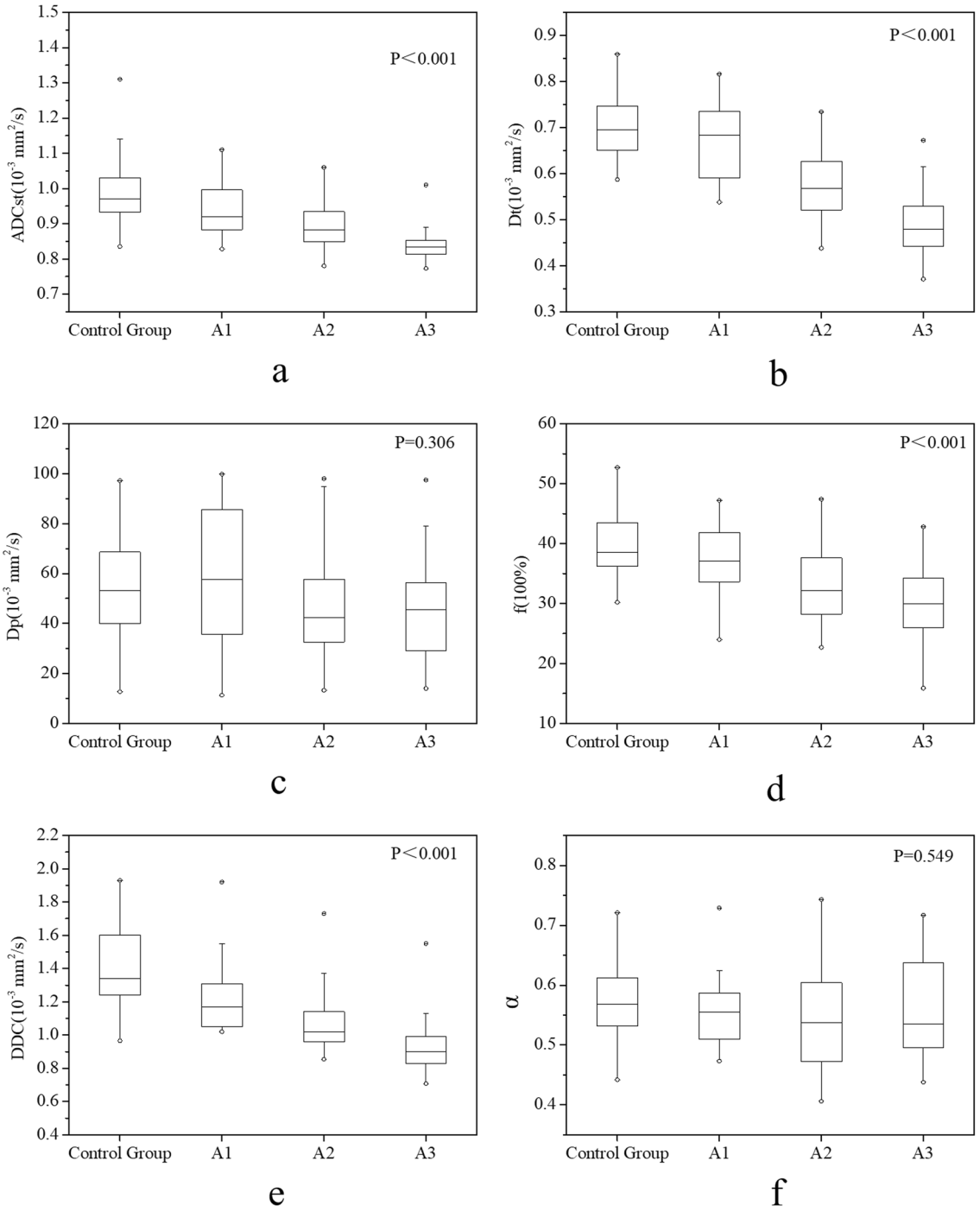

Fig. 4 Box plots of ADC_{st} values (**a**), D_t values (**b**), D_p values (**c**), f values (**d**), DDC values (**e**), and α values (**f**) in the control group and groups A1, A2, and A3. ADC_{st}, D_t, f, and DDC were significantly different among the above groups (all $P < 0.001$). However, D_p and α did not show significant differences (all $P > 0.05$)

with a fast flow which is measured with b-values lower than 200 s/mm^2, and f is used for reflecting the fraction of flowing blood in the capillaries [11, 13, 15–20, 27]. Several prior studies [10, 24, 25, 28] have reported that D_p values were significantly lower in the fibrotic or cirrhotic liver group than in the control group. Interestingly, in our study, the D_p values showed no significant difference among the control and fibrosis groups. We believe that the inconsistencies between the results of our study and the prior studies were caused by the following factors: first, in our study, very low b-values

Table 1 Comparisons of the diffusion parameters between fibrosis stages

Parameter	≤F1 and ≥F2		*P*	≤F2 and ≥F3		*P*	≤F3 and F4		*P*
	Mean ± SD			Mean ± SD			Mean ± SD		
ADC_{st} *	0.92 ± 0.08	0.88 ± 0.07	0.029	0.91 ± 0.08	0.86 ± 0.05	0.001	0.90 ± 0.07	0.84 ± 0.03	< 0.001
D_t*	0.67 ± 0.08	0.55 ± 0.08	< 0.001	0.62 ± 0.08	0.50 ± 0.07	< 0.001	0.60 ± 0.09	0.47 ± 0.06	< 0.001
D_p*	54.91 ± 29.85	46.27 ± 21.05	0.348	51.02 ± 25.07	43.88 ± 19.91	0.314	50.14 ± 24.32	38.77 ± 14.67	0.159
f(%)	37.32 ± 6.92	31.83 ± 6.46	0.008	34.94 ± 6.77	30.18 ± 6.12	0.004	34.15 ± 6.50	27.69 ± 6.24	0.001
DDC*	1.23 ± 0.25	1.03 ± 0.19	< 0.001	1.16 ± 0.22	0.95 ± 0.15	< 0.001	1.11 ± 0.22	0.88 ± 0.10	< 0.001
α	0.56 ± 0.06	0.55 ± 0.09	0.482	0.56 ± 0.08	0.55 ± 0.10	0.522	0.55 ± 0.08	0.57 ± 0.10	0.385

*Values are in units of $\times 10^{-3}$ mm^2/s

($0 < b < 50$ s/mm^2) were not included in the *b*-value distribution, which may have resulted in underestimation of D_p at the lower *b*-values of 0, 50, 100, and 150 s/mm^2. Second, the instability and the large SD of D_p could have influenced the findings [29–31]. Third, the HF samples in each stage were different, and the patient populations varied. The *f* values from the biexponential model reflect the fast diffusion fraction caused by microcirculatory blood perfusion and account for the ratio of the total diffusion components (including fast and slow diffusion). Our study revealed that the *f* value in the control group were higher than the *f* values in the HF groups. This finding was consistent with the results from some prior studies [10, 23].

Previous studies [3, 10] have reported that patients with fibrosis stage ≤ F1 have a low risk of liver failure, while stage ≥ F2 is a predictor of future hepatic cirrhosis and is an indication for therapy. In addition, patients with stage ≥ F3 require screening for portal hypertension and HCC. In our study, the D_t outperformed the ADC_{st} in diagnosing fibrosis stage ≥ F2, ≥ F3. This could be attributed to the fact that D_t can basically eliminate the influence of microcirculation perfusion and can more accurately reflect the diffusion limitation of water molecules. However, the ADC_{st} value was affected by the microcirculation perfusion when reflecting the diffusion of water molecules, thereby showing slightly inferior efficacy and accuracy for diagnosis of HF. Besides, our study also showed that DDC outperformed ADC_{st} with good diagnostic performance in detecting fibrosis stages ≥ F2 and ≥ F3. This could be attributed to the fact that DDC is a weighted sum over a continuous allocation of ADC_{st} values and reflect the multi-exponential decay properties [12, 32]. Therefore, based on the study results, we believe that D_t and DDC could be more beneficial than ADC_{st} for diagnosing significant HF(≥ F2) and advanced fibrosis(≥ F3) and the superior performance of D_t and DDC compared with that of ADC_{st} can have clinically important value for managing patients with HF. Thus, we assume that D_t, DDC could be used to determine the indication of antifibrotic treatment and as a marker for monitoring progression, and evaluating treatment efficacy.

HF is known to be accompanied by varying degrees of inflammation. Since inflammatory activity is closely related to the progression and prognosis of HF, assessment of the extent of inflammation is also very important [33]. In the process of chronic hepatitis, oedema, degeneration, and necrosis of liver cells and infiltration of inflammatory cells in the portal area and lobules may decrease the extracellular/liquid volume ratio in the cell, cause liver tissue ischaemia, and reduce liver tissue blood flow. Therefore, the presence of inflammation in chronic hepatitis may cause limited water-molecule diffusion and decreased blood perfusion in the liver. Moreover, an increase in inflammatory activity can further limit water-molecule diffusion and reduce hepatic tissue perfusion. The results of our study showed that ADC_{st}, D_t, DDC, and *f* values in the inflammatory activity grade groups (A1, A2, and A3) were significantly lower than the corresponding parameters in the control group. Additionally, the mean ADC_{st}, D_t, DDC, and *f* values in the groups decreased gradually. These current findings were consistent with the results from prior studies [6, 26]. Thus, the ADC_{st}, D_t, DDC, and *f* values of the liver may reflect the extent of inflammatory activity.

It is widely accepted that patients with inflammatory activity ≥ A2 are at a higher risk of developing liver cirrhosis and need to receive antiviral treatment [34]. Thus, we believe that accurate diagnosis of inflammatory activity ≥ A2 may have significant clinical implications. In the study, D_t, DDC and ADC_{st} all showed moderate diagnostic performance for detecting inflammatory activity ≥ A2 and A3 (AUC:0.7–0.9) and had comparable diagnostic performance in detecting grade ≥ A2/A3. Thus, we believe that D_t, DDC and ADC_{st} could be used to determine the indication of antiviral treatment and as a marker for therapy surveillance.

This study had some limitations. First, the number of patients was relatively small, and the distributions of fibrosis stages and inflammatory activity grades were uneven. Second, the influence of iron or fat deposition in HF on the diffusion parameters was not assessed. Third, D_p values might have been underestimated at the lower *b*-values of 0, 50, 100, and 150 s/mm^2 since very low *b*-values ($0 < b < 50$ s/mm^2)

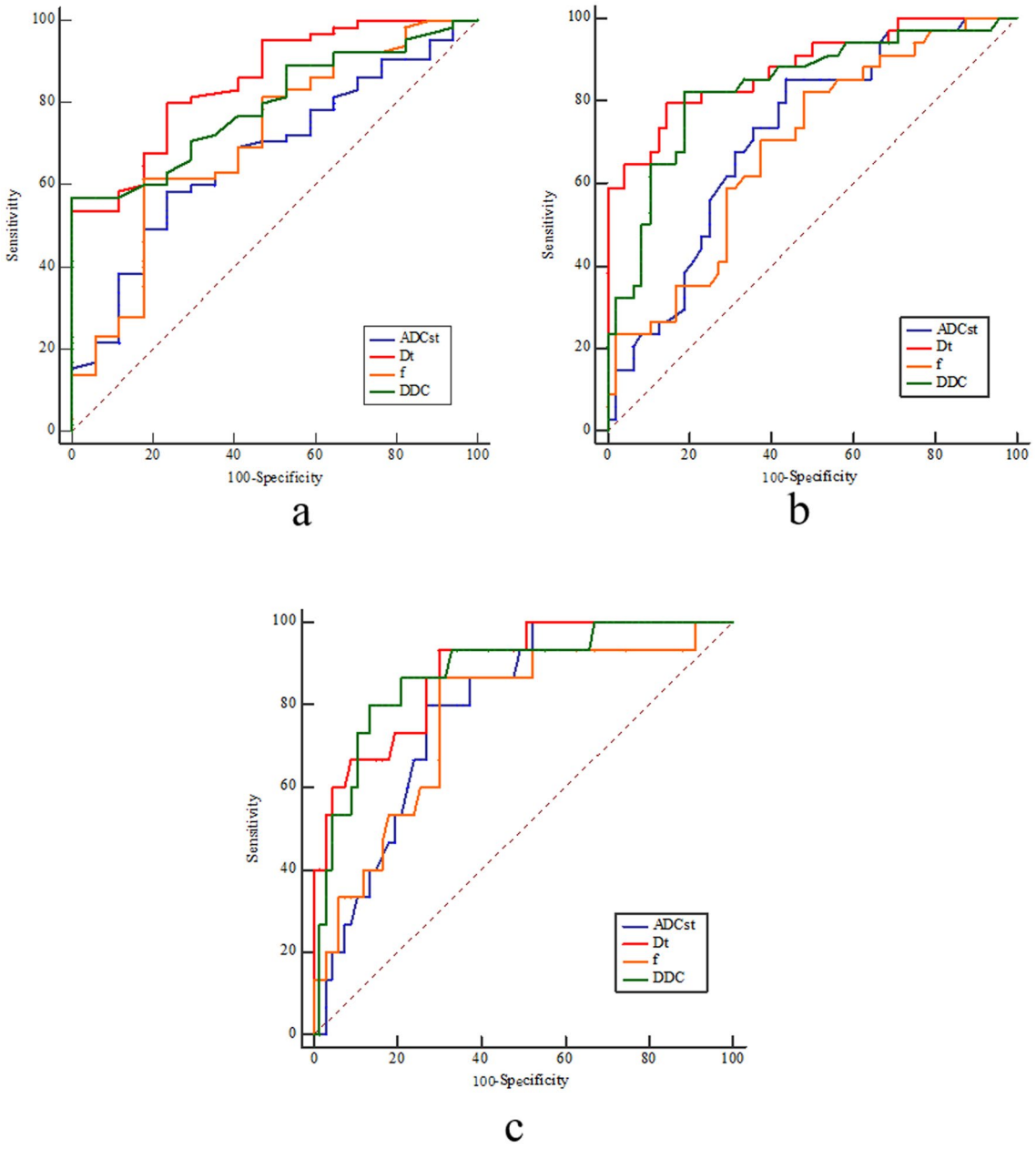

Fig. 5 ROC curves for ADC_{st}, D_t, f and DDC in distinguishing ≥F2 from ≤F1 (**a**). ROC curves for ADC_{st}, D_t, DDC and f in distinguishing ≥F3 from ≤F2 (**b**). ROC curves for ADC_{st}, D_t, f and DDC in distinguishing F4 from ≤F3 (**c**)

were not selected. Finally, the liver diffusion parameters in patients with CHB were determined by both fibrosis stage and inflammatory activity grade, but it is unclear which aspect has a greater role, and further stratified research is required to address this issue.

In conclusion, the D_t derived from the biexponential model and DDC from the stretched-exponential model are more valuable than other parameters in predicting significant fibrosis, advanced fibrosis in patients with CHB. Therefore, we believe that D_t and DDC could be used clinically to diagnose and stage HF, and as a marker for guiding therapy, monitoring progression, and evaluating treatment efficacy in a noninvasive manner.

Table 2 Performance of diffusion parameters in predicting fibrosis stage

	Parameter	AUC	95% CI	Cutoff values	Sensitivity (%)	Specificity (%)
≥F2	ADC_{st}*	0.673	0.560–0.772	0.875	58.5	76.5
	D_t*	0.854	0.759–0.922	0.615	80	76.5
	f(%)	0.711	0.601–0.806	32.80	82.4	61.5
	DDC*	0.794	0.691–0.876	1.000	56.9	100
≥F3	ADC_{st}*	0.717	0.607–0.811	0.891	85.3	56.3
	D_t*	0.881	0.790–0.942	0.537	79.4	85.4
	f(%)	0.689	0.577–0.786	35.6	82.4	52.1
	DDC*	0.834	0.736–0.907	1.00	82.4	81.3
F4	ADC_{st}*	0.791	0.687–0.873	0.853	80.0	73.1
	D_t*	0.886	0.796–0.945	0.537	93.3	70.2
	f(%)	0.768	0.662–0.854	30.00	86.7	70.2
	DDC*	0.878	0.787–0.940	0.921	80	86.6

*Values are in units of $\times 10^{-3}$ mm^2/s

Table 3 Comparisons of the diffusion parameters between inflammatory activity grades

Parameter	≤A1 and ≥A2		*P*	≤A2 and ≥A3		*P*
	Mean ± SD			Mean ± SD		
ADC_{st}*	0.95 ± 0.08	0.88 ± 0.07	0.001	0.91 ± 0.07	0.84 ± 0.05	< 0.001
D_t*	0.68 ± 0.08	0.55 ± 0.08	< 0.001	0.60 ± 0.09	0.49 ± 0.07	< 0.001
D_p*	58.15 ± 29.21	45.80 ± 21.25	0.150	49.27 ± 23.79	44.53 ± 21.59	0.483
f	37.45 ± 6.70	31.96 ± 6.56	0.009	34.02 ± 6.64	29.89 ± 6.83	0.024
DDC*	1.25 ± 0.25	1.03 ± 0.19	< 0.001	1.12 ± 0.21	0.93 ± 0.18	< 0.001
α	0.56 ± 0.06	0.56 ± 0.09	0.890	0.56 ± 0.08	0.56 ± 0.09	0.828

*Values are in units of $\times 10^{-3}$ mm^2/s

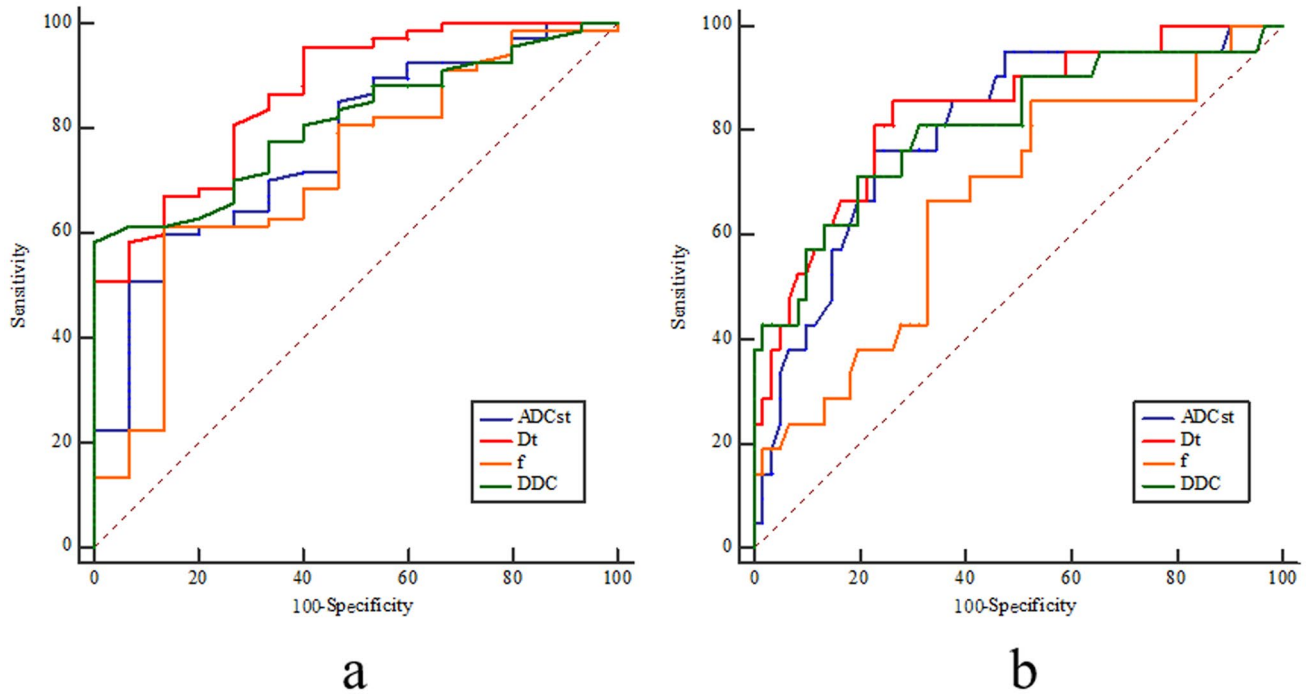

Fig. 6 ROC curves for ADC_{st}, D_t, *f*, and DDC in distinguishing ≥A2 from ≤A1 (**a**). ROC curves for ADC_{st}, D_t, *f*, and DDC in distinguishing A3 from ≤A2 (**b**)

Table 4 Performance of diffusion parameters in predicting inflammatory activity grade

	Parameter	AUC	95% CI	Cutoff values	Sensitivity (%)	Specificity (%)
≥ A2	ADC_{st}*	0.767	0.661–0.853	0.875	59.7	86.7
	D_t*	0.867	0.774–0.932	0.679	95.5	60.0
	f(%)	0.717	0.607–0.811	32.85	61.2	86.7
	DDC*	0.810	0.709–0.889	1.010	58.2	100
A3	ADC_{st}*	0.803	0.700–0.883	0.853	76.2	77.0
	D_t*	0.836	0.738–0.908	0.537	85.7	73.8
	f(%)	0.665	0.553–0.766	30.10	66.7	67.2
	DDC*	0.808	0.706–0.887	0.969	71.4	80.3

*Values are in units of $\times 10^{-3}$ mm^2/s

Acknowledgements This work was supported by National Natural Science Foundation of China (Grant Nos. 81720108021, 81601466, 81641168, 31470047, and 81271534).

Compliance with ethical standards

Conflict of interest All authors declare that they have no conflicts of interest.

References

1. Schweitzer A, Horn J, Mikolajczyk RT, Krause G, Ott JJ (2015) Estimations of worldwide prevalence of chronic hepatitis B virus infection: a systematic review of data published between 1965 and 2013. Lancet 386: 1546–1555. https://doi.org/10.1016/s0140-6736(15)61412-x
2. Maini K, Pallet JD (2018) T-cell immunity in hepatitis B virus infection: why therapeutic vaccination needs a helping hand. Lancet Gastroenterol Hepatol 3: 192–202. https://doi.org/10.1016/S2468-1253(18)30007-4
3. The Polaris Observatory Collaborators (2018) Global prevalence, treatment, and prevention of hepatitis B virus infection in 2016: a modelling study. Lancet Gastroenterol Hepatol 3:383–403. https://doi.org/10.1016/s2468-1253(18)30056-6
4. Friedman SL (2003) Liver fibrosis—from bench to bedside. J Hepatol 38: S38–S53. https://doi.org/10.1016/s0168-8278(02)00429-4
5. Manning DS, Afdhal NH (2008) Diagnosis and quantitation of fibrosis. Gastroenterology 134: 1670–1681. https://doi.org/10.1053/j.gastro.2008.03.001
6. Fujimoto K, Tonan T, Azuma S, et al. (2011) Evaluation of the Mean and Entropy of Apparent Diffusion Coefficient Values in Chronic Hepatitis C: Correlation with Pathologic Fibrosis Stage and Inflammatory Activity Grade. Radiology 258: 739–748. https://doi.org/10.1148/radiol.10100853
7. Standish RA, Cholongitas E, Dhillon A, Burroughs AK, Dhillon AP (2006) An appraisal of the histopathological assessment of liver fibrosis. Gut 55: 569–578. https://doi.org/10.1136/gut.2005.084475
8. Sandrasegaran K, Akisik FM, Lin C, et al. (2009) Value of diffusion-weighted MRI for assessing liver fibrosis and cirrhosis. AJR Am J Roentgenol 193: 1556–60. https://doi.org/10.2214/ajr.09.2436
9. Taouli B, Koh DM (2010) Diffusion-weighted MR imaging of the liver. Radiology 254: 47–66. https://doi.org/10.1148/radiol.09090021
10. Yoon JH, Lee JM, Baek JH, et al. (2014) Evaluation of hepatic fibrosis using intravoxel incoherent motion in diffusion-weighted liver MRI. J Comput Assist Tomogr 38: 110–116. https://doi.org/10.1097/rct.0b013e3182a589be
11. Bihan DL, Breton E, Lallemand D, et al. (1986) MR imaging of intravoxel incoherent motions: application to diffusion and perfusion in neurologic disorders. Radiology 161: 401–407. https://doi.org/10.1148/radiology.161.2.3763909
12. Bennett KM, Schmainda KM, Bennett RT, et al. (2003) Characterization of continuously distributed cortical water diffusion rates with a stretched-exponential model. Magn Reson Med 50: 727–734. https://doi.org/10.1002/mrm.10581
13. Bihan De, Breton E, Lallemand D, et al. (1988) Separation of diffusion and perfusion in intravoxel incoherent motion MR imaging. Radiology 168: 497–505. https://doi.org/10.1148/radiology.168.2.3393671
14. Bennett KM, Hyde JS, Schmainda KM (2006) Water diffusion heterogeneity index in the human brain is insensitive to the orientation of applied magnetic field gradients. Magn Reson Med 56: 235–239. https://doi.org/10.1002/mrm.20960
15. Santis SD, Gabrielli A, Palombo M, Maraviglia B, Capuani S (2011) Non-Gaussian diffusionimaging: a brief practical review. Magn Reson Imaging 29: 1410–1416. https://doi.org/10.1016/j.mri.2011.04.006
16. Sandrasegaran K, Territo P, Elkady RM, et al. (2018) Does intravoxel incoherent motion reliably stage hepatic fibrosis, steatosis, and inflammation? Abdom Radiol 43:600–606. https://doi.org/10.1007/s00261-017-1263-8
17. Liu X, Zhou L, Peng W, Wang H, Zhang Y (2015) Comparison of stretched-exponential and monoexponential model diffusion-weighted imaging in prostate cancer and normal tissues. J Magn Reson Imaging 42: 1078–1085. https://doi.org/10.1002/jmri.24872
18. Seo N, Chung YE, Park YN, et al. (2018) Liver fibrosis: stretched exponential model outperforms mono-exponential and bi-exponential models of diffusion-weighted MRI. Eur Radiol 28:1–11. https://doi.org/10.1007/s00330-017-5292-z
19. Chung S, Lee SS, Kim N, et al. (2015) Intravoxel incoherent motion MRI for liver fibrosis assessment: a pilot study. Acta Radiol 56: 1428–1436. https://doi.org/10.1177/0284185114559763
20. Franca M, Marti-Bonmati L, Alberich-Bayarri A, et al. (2017) Evaluation of fibrosis and inflammation in diffuse liver diseases using intravoxel incoherent motion diffusion-weighted

MR imaging. Abdom Radiol (NY) 42:468–477. https://doi.org/10.1177/0284185114559763
21. Watanabe H, Kanematsu M, Goshima S, et al. (2011) Staging hepatic fibrosis: comparison of gadoxetate disodium-enhanced and diffusion-weighted MR imaging-preliminary observations. Radiology 259:142–150. https://doi.org/10.1148/radiol.10100621
22. Bedossa P, Poynard T (1996) An algorithm for the grading of activity in chronic hepatitis C. The METAVIR Cooperative Study Group. Hepatology 24:289–293. https://doi.org/10.1002/hep.510240201
23. Friedman SL (2000) Molecular regulation of hepatic fibrosis, an integrated cellular response to tissue injury. J Biol Chem 275:2247–2250. https://doi.org/10.1074/jbc.275.4.2247
24. Patel J, Sigmund EE, Rusinek H, et al. (2010) Diagnosis of cirrhosis with intravoxel incoherent motion diffusion MRI and dynamic contrast-enhanced MRI alone and in combination: preliminary experience. J Magn Reson Imaging 31: 589–600. https://doi.org/10.1002/jmri.22081
25. Luciani A, Vignaud A, Cavet M, et al. (2008) Liver cirrhosis: intravoxel incoherent motion MR imaging-pilot study. Radiology 249:891–899. https://doi.org/10.1148/radiol.2493080080
26. Anderson SW, Barry B, Soto J, et al. (2014) Characterizing non-Gaussian, high b-value diffusion in liver fibrosis: stretched exponential and diffusional kurtosis modeling [J]. J Magn Reson Imaging 39: 827–834. https://doi.org/10.1002/jmri.24234
27. Gulbay M, Ciliz DS, Celikbas AK, et al. (2020) Intravoxel incoherent motion parameters in the evaluation of chronic hepatitis B virus-induced hepatic injury: fibrosis and capillarity changes. Abdom Radiol (NY) 45(8):2345–2357. https://doi.org/10.1007/s00261-020-02430-9
28. Chow AM, Gao DS, Fan SJ, et al. (2012) Liver fibrosis: an intravoxel incoherent motion (IVIM) study. J Magn Reson Imaging 36:159–167. https://doi.org/10.1002/jmri.23607
29. Winfield JM, Desouza NM, Priest AN, et al. (2015) Modelling DW-MRI data from primary and metastatic ovarian tumours. Eur Radiol 25:2033–2040. https://doi.org/10.1007/s00330-014-3573-3
30. Cohen AD, Schieke MC, Hohenwalter MD,Schmainda KM (2015) The effect of low b-values on the intravoxel incoherent motion derived pseudo diffusion parameter in liver. Magn Reson Med 73: 306–311. https://doi.org/10.1002/mrm.25109
31. Sigmund EE, Vivier PH, Sui D, et al. (2012) Intravoxel incoherent motion and diffusion-tensor imaging in renal tissue under hydration and furosemide flow challenges. Radiology 263: 758–769. https://doi.org/10.1148/radiol.12111327
32. Bai Y, Lin Y, Tian J, et al. (2016) Grading of gliomas by using monoexponential, biexponential, and stretched exponential diffusion-weighted MR imaging and diffusion kurtosis MR imaging. Radiology 278: 496–504. https://doi.org/10.1148/radiol.2015142173
33. Guido M, Fagiuoli S, Tessari G, et al. (2002) Histology predicts cirrhotic evolution of post-transplant hepatitis C. Gut 50: 697–700. https://doi.org/10.1136/gut.50.5.697
34. Tang CM, Yau TO, Yu J, (2014) Management of chronic hepatitis B infection: current treatment guidelines, challenges, and new developments. World J Gastroenterol 20: 6262–78. https://doi.org/10.3748/wjg.v20.i20.6262